arXiv:1701.04232v1 [cond-mat.stat-mech] 16 Jan 2017

Hierarchy of the low-lying excitations for the $(2+1)$-dimensional $q=3$ Potts model in the ordered phase

Yoshihiro Nishiyama

Department of Physics, Faculty of Science, Okayama University, Okayama 700-8530, Japan

Abstract

The $(2+1)$-dimensional $q=3$ Potts model was simulated with the exact diagonalization method. In the ordered phase, the elementary excitations (magnons) are attractive, forming a series of bound states in the low-energy spectrum. We investigate the low-lying spectrum through a dynamical susceptibility, which is readily tractable with the exact diagonalization method via the continued-fraction expansion. As a result, we estimate the series of (scaled) mass gaps, $m_{2,3,4}/m_1$ (m_1: single-magnon mass), in proximity to the transition point.

Keywords:

75.10.Jm 75.40.Mg 05.50.+q , 05.70.Jk

1. Introduction

In the ordered phase for an Ising ferromagnet, the elementary excitations (magnons) are attractive, forming a series of bound states (composite particles) with the mass gaps, $m_1 < m_2 < \ldots$ (m_1: single-magnon mass). In fact, for the $(1+1)$-dimensional Ising model [1, 2, 3], there appear eight types of excitations with the (scaled) mass gaps

$$m_2/m_1 = 2\cos\pi/5 \quad (1)$$

$$m_3/m_1 = 2\cos\pi/30 \quad (2)$$

$$m_4/m_2 = 2\cos 7\pi/30 \quad (3)$$

$$m_5/m_2 = 2\cos 2\pi/15 \quad (4)$$

$$m_6/m_2 = 2\cos\pi/30 \quad (5)$$

$$m_7/m_2 = 4\cos\pi/5\cos 7\pi/30 \quad (6)$$

$$m_8/m_2 = 4\cos\pi/5\cos 2\pi/15, \quad (7)$$

under a properly scaled magnetic field so as to preserve the integrability; namely, the scaled gap ratio, $m_{2,3,\ldots}/m_1$, displays a universal hierarchical character. For a quasi-one-dimensional ferromagnet, $CoNb_2O_6$, the primary one, $m_2/m_1 = 1.61\ldots$ (golden ratio), was confirmed by means of the inelastic neutron scattering [4]. For the $(2+1)$-dimensional counterpart, such rigorous information is not available, and various approaches have been made so as to fix the hierarchical structure $m_{2,3,\ldots}/m_1$ [5, 6, 7, 8, 9, 10, 11, 12]. Meanwhile, it turned out that the spectrum for the three-state ($q = 3$) Potts model exhibits a hierarchical character as well [13, 14, 15, 16, 17, 18]. Related results are recalled afterwards.

According to the Monte Carlo simulations in $(2+1)$ dimensions [18, 19], the hierarchy $m_{1,2,\ldots}$ of the Potts model and that of the pure gauge theory look alike. Actually, for the Z_2 case in $(2+1)$ dimensions, a duality relation [20, 21, 22] does hold, ensuring the correspondence between them. Generically [23], the SU(N) gauge theory displays a global Z_N symmetry (center of SU(N)), which immediately establishes a relationship between them; for $N \geq 3$, the transition would not be critical, and the universality idea does not apply nonetheless. Meanwhile, an extensive lattice-gauge-theory simulation reveals the "weak N dependence" [24] of the SU(N) theory, suggesting a robustness of the hierarchy, $m_{2,3,\ldots}/m_1$. On the one hand, the $q = 3$ Potts model exhibits an "approximate universality" [25], even though the phase transition is of first order. Hence, it is expected that the hierarchy should display a model-independent character to some extent.

In this paper, we investigate the $(2+1)$-dimensional $q = 3$ Potts model [26, 27] by means of the numerical diagonalization method. The method allows us to evaluate the dynamical susceptibilities, Eqs. (12) and (17), via the continued-fraction-expansion method [28]. In Fig. 1, we present a schematic drawing for a spectral function.

To be specific, we present the Hamiltonian for the $(2+1)$-dimensional $q=3$ Potts model

$$\mathcal{H} = -\sum_{\langle ij \rangle} \frac{2}{3} \cos\left(\frac{2\pi}{3}(L_i - L_j)\right) - \lambda \sum_{i=1}^{N} (R_i^+ + R_i^-) - H \sum_{i=1}^{N} \frac{2}{3} \cos\frac{2\pi L_i}{3}. \quad (8)$$

Here, the operator

$$L_i = \begin{pmatrix} 0 & 0 & 0 \\ 0 & 1 & 0 \\ 0 & 0 & 2 \end{pmatrix}, \quad (9)$$

is placed at each square-lattice point $i = 1, 2, \ldots, N$; namely, the base $|l_i\rangle$ ($l_i = 0, 1, 2$) satisfies $L_i|l_i\rangle = l_i|l_i\rangle$. The summation $\sum_{\langle ij \rangle}$ runs over all possible nearest neighbor pairs $\langle ij \rangle$. The operator $R_i^{\pm}$ induces the transition $R_i^{\pm}|l_i\rangle = |l_i \pm 1 \bmod 3\rangle$, and the parameter λ denotes the corresponding coupling constant. This model exhibits the first-order phase transition at $\lambda = \lambda_c = 0.8758(14)$ ($H = 0$) [25], which separates the ordered ($\lambda < \lambda_c$) and disordered ($\lambda > \lambda_c$) phases. An infinitesimal magnetic field $H = 20/L^{2.5}$ (L: linear dimension of the finite-size cluster) stabilizes [3] the ground state, and the power 2.5 comes from the putative scaling theory [26] for the $(2+1)$-dimensional $q=3$ Potts model. Note that the first-order phase transition also obeys the remedied scaling theory [29, 30, 31, 32].

The rest of this paper is organized as follows. In the next section, we present the numerical results. The simulation algorithm is presented as well. In Sec. 3, we address the summary and discussions.

2. Numerical results

In this section, we present the numerical results for the Potts model (8). To begin with, we explain the simulation algorithm.

2.1. Numerical algorithm

We employed the exact diagonalization method to simulate the Potts model (8) for a rectangular cluster with $N \leq 22$ spins. In order to treat a variety of

$N = 16, 18, \ldots$ systematically, we implemented the screw-boundary condition [33]. According to Ref. [33], an alignment of spins $\{l_i\}$ with the first- and $\sqrt{N}$-th-neighbor interactions reduces to a rectangular cluster under the screw-boundary condition. Based on this idea, we express the Hamiltonian as

$$\mathcal{H} = H_D(1) + H_D\left(\sqrt{N}\right) - \lambda \sum_{i=1}^{N} (R_i^+ + R_i^-) - H \sum_{i=1}^{N} \frac{3}{2} \cos \frac{2\pi L_i}{3}. \qquad (10)$$

Here, the diagonal matrix $H_D(v)$ denotes the v-th-neighbor interaction for an alignment $\{l_i\}$; that is, the diagonal element is given by $\langle\{l_i\}|H_D(v)|\{l_i\}\rangle = \langle\{l_i\}|TP^v|\{l_i\}\rangle$ with the translation operator, $P|\{l_i\}\rangle = |\{l_{i+1}\}\rangle$, and the Potts interaction, $\langle\{l_i\}|T|\{l_i'\}\rangle = -\sum_{i=1}^{N} \delta_{l_i,l_i'}$. The above formulae are mathematically closed; however, for an efficient simulation, Eqs. (9) and (10) of Ref. [34] may be of use.

We performed the numerical diagonalization for the Hamiltonian matrix (10) by means of the Lanczos method. The single-magnon mass gap m_1 is given by

$$m_1 = E_1 - E_0, \qquad (11)$$

with the ground-state (E_0) and first-excited (E_1) energy levels within the zero-momentum sector. Because the N spins form a rectangular cluster, the linear dimension is given by $L = \sqrt{N}$, which sets a foundermental length scale in the subsequent scaling analyses.

2.2. Single-magnon mass gap m_1

In this section, we investigate the single-magnon mass gap m_1 (11) with the scaling theory [26, 31]. The first-order phase transition obeys the properly remedied scaling theory.

In Fig. 2, we present the scaling plot, $(\lambda - \lambda_c)L^{1/\nu}$-$m_1/m_{1c}$, for (+) $N = 16$, ($\times$) 18, ($*$) 20, and ($\Box$) 22. Here, the symbol m_{1c} denotes $m_{1c} = m_1|_{\lambda=\lambda_c}$ [31], and the scaling parameters, $\lambda_c = 0.8758$ and $\nu = 0.5$, are taken from Refs. [25] and [26, 31], respectively. We stress that there is no *ad hoc* fitting parameter involved in the scaling analysis.

The data in Fig. 2 seem to collapse into a scaling curve, indicating that the simulation data already enter the scaling regime. Encouraged by this finding, we turn to the analysis of the spectral properties.

2.3. Hierarchical spectral peaks $m_{2,3,...}$ via $\chi''_A(\omega)$

Based on the finite-size scaling [26, 31] demonstrated in the preceding section, we analyze the dynamical susceptibility

$$\chi''_A(\omega) = -\Im\langle 0|A^\dagger(\omega + E_0 - \mathcal{H} + \mathrm{i}\eta)^{-1}A|0\rangle, \tag{12}$$

with the ground-state energy (vector) E_0 ($|0\rangle$) and the energy-resolution parameter η. Here, the perturbation operator is set to

$$A = \mathcal{P}\left(\sum_{i=1}^{N} J_i\right)^2, \tag{13}$$

with

$$J_i = \begin{pmatrix} 0 & \mathrm{i} & \mathrm{i} \\ -\mathrm{i} & 0 & 0 \\ -\mathrm{i} & 0 & 0 \end{pmatrix}, \tag{14}$$

and the projection operator $\mathcal{P} = 1 - |0\rangle\langle 0|$. We calculated the dynamical susceptibility (12) with the continued-fraction expansion [28]. The dynamical susceptibility (spectral function) obeys the scaling formula

$$\chi''_A \sim L^5 f(\omega/m_1, (\lambda - \lambda_c)L^{1/\nu}), \tag{15}$$

with a certain scaling function f [35, 12].

In Fig. 4, we present the scaling plot, ω/m_1-$L^{-5}\chi''_A(\omega)$, with fixed $(\lambda - \lambda_c)L^{1/\nu} = -4$ and $\eta = 0.1m_1$ for various $N = 18$ (dotted), 20 (solid), and 22 (dashed); here, the scaling parameters, λ_c and ν, are the same as those of Fig. 2. The data appear to collapse into a scaling curve satisfactorily.

Each signal in Fig. 3 is interpreted by the diagram in Fig. 1. That is, the peaks around $\omega/m_1 \approx 1.8$, 2.5 and 3 correspond to the $m_{2,3,4}$ excitations, respectively. The shoulder peak around $\omega/m_1 \approx 2$ should be the two-magnon-spectrum threshold. The signal $\omega/m_1 \approx 3.5$ may be either the m_5 particle or a

composite one consisting of m_1 and m_2. The ratios $m_{2,3,4}/m_1$ are estimated in the next section more in detail.

Last, we mention the choice of the perturbation operator A (13). In a preliminary stage, we surveyed various types of the perturbation operators, aiming to create the $m_{2,3,...}$ particles effectively. Actually, neither the first or the second term of the Hamiltonian (8) commutes with A; otherwise, the susceptibility reduces to a mere specific heat. A key ingredient is that the exact diagonalization method permits us to treat any off-diagonal operators.

2.4. Universality of the scaled masses $m_{2,3,4}/m_1$

In this section, we devote ourselves to the analysis of the scaled masses $m_{2,3,4}/m_1$; it is expected that each ratio takes a constant value in proximity to the transition point [25].

In Fig. 4, we present the scaling plot, ω/m_1-$L^{-5}\chi''_A(\omega)$, with fixed $N = 22$ and $\eta = 0.1m_1$ for various values of the scaling parameter, $(\lambda - \lambda_c)L^{1/\nu} = -3$ (dotted), -4 (solid), and -5 (dashes); the scaling parameters, λ_c and ν, are the same as those of Fig. 2. Note that these curves do not necessarily overlap, because the scaling parameter $(\lambda-\lambda_c)L^{1/\nu}$ is not a constant value; see Eq. (15) for the scaling formula. Each peak position seems to be kept invariant, albeit with the scaling parameter varied. As a result, we estimate the scaled mass gaps as

$$(m_2/m_1, m_3/m_1, m_4/m_1) = [1.80(3), 2.5(1), 3.05(25)]. \tag{16}$$

Here, each error margin was determined from the finite-size drift between $N = 16$ and 20; a dominant source of the error margin comes from the oscillatory deviation (an artifact due to the screw-boundary condition), which depends on the condition whether the system size is a quadratic number $N \sim 9, 16, \ldots$ or not $N \sim 12(\approx 3.5^2), 20(\approx 4.5^2), \ldots$.

Each particle $m_{3,4}$ may possess a finite life time, because it is embedded within the two-particle spectrum. As a matter of fact, the data for $(\lambda - \lambda_c)L^{1/\nu} = -3$ (dotted) in Fig. 4 exhibit split peaks around $\omega/m_1 \approx 2.5$, indicating that the bound state m_3 has an appreciable peak width, $\Delta m_3/m_1 =$

0.3. Similarly, we observed $\Delta m_4/m_1 = 0.35$ for the data with $N = 18$ and $(\lambda - \lambda_c)L^{1/\nu} = -6$. To summarize, we estimate the intrinsic peak widths (reciprocal life time) as $\Delta m_3/m_1 = 0.3$ and $\Delta m_4/m_1 = 0.35$. Each peak width is about one tenth of the corresponding mass gap.

This is a good position to address an overview of the related studies. First, for the classical three-dimensional $q = 3$ Potts model, an estimate $m_{2^+}/m_{0^+} = 2.43(10)$ [18] was reported; the notation (symmetry index) is taken from the original paper. This result may correspond to the present result, $m_3/m_1 = 2.5(1)$, Eq. (16), supporting an "approximate universality" [25] for the $q = 3$ Potts model. Second, as for the Z_2 [36] and SU(2) [37] gauge field theories, the results, $(m_{(0^+)'}/m_{0^+}, m_{(0^+)''}/m_{0^+}, m_{(2^+)'}/m_{0^+}) = [1.88(2), 2.59(4), 3.23(7)]$ and $(m_{(0^+)'}/m_{0^+}, m_{(0^+)''}/m_{0^+}, m_{2^+}/m_{0^+}) = [1.89(16), 2.35(10), 3.36(40)]$, respectively, were obtained. The hierarchical structures are quite reminiscent of ours, Eq. (16). As a matter of fact, for the gauge field theory, the "week N dependence" of the gauge group SU(N) was reported [24], indicating a robustness of the hierarchy $m_{2,3,\ldots}/m_1$. For the SU(3) gauge field [19], a glueball mass, either $m_{2^+}/m_{0^+} = 3.214(64)$ or 3.172(65), was estimated. The result may correspond to $m_4/m_1 = 3.05(25)$, Eq. (16). Last, for the Ising model [5, 6, 7, 8, 9, 10, 11, 12], estimates, $m_2/m_1 = 1.82(2)$ [11] and $m_3/m_1 = 2.45(10)$ [5], were reported. These results resemble to ours, Eq. (16), supporting a model-independence on the hierarchy.

Last, we address a remark. Because the phase transition is discontinuous, the continuum limit cannot be taken properly. The above estimates such as the life time are specific to a lattice realization, although seemingly preferable scaling behavior was observed. However, in an approximate sense, the simulation results seem to be comparable with the related ones, as claimed by the preceeding studies [18, 19, 25].

2.5. Continuum-threshold peak via $\chi''_B(\omega)$

As a comparison, we present a simulation result for χ''_B (17), aiming to see to what extent the spectral weight is affected by the choice of the perturbation

operator. The dynamical susceptibility χ''_B is defined by

$$\chi''_B(\omega) = -\Im\langle 0|B^\dagger(\omega + E_0 - \mathcal{H} + \mathrm{i}\eta)^{-1}B|0\rangle, \tag{17}$$

with a perturbation operator

$$B = \mathcal{P}\sum_{i=1}^{N}(R_i^+ + R_i^-). \tag{18}$$

Note that the operator B coincides with the second term of the Hamiltonian (8). Hence, it exhibits the specific-heat-type singularity $\chi''_B \sim L^{2/\nu-1}$ with $\nu = 0.5$ [26, 31] right at the transition point.

In Fig. 5, we present the scaling plot, ω/m_1-$L^{-3}\chi''_B(\omega)$, with fixed $(\lambda - \lambda_c)L^{1/\nu} = -4$ and $\eta = 0.1m_1$ for various $N = 18$ (dots), 20 (solid), and 22 (dashed); the scaling parameters, λ_c and ν, are the same as those of Fig. 2. In contrast with χ''_A in Fig. 3, the susceptibility χ''_B detects the $m_{1,2}$ signals and the two-magnon-spectrum-threshold peak $\omega/m_1 \approx 2$; instead, the bound-state hierarchy $m_{3,4}$ becomes hardly observable.

The result indicates that a naive external disturbance such as the specific-heat-type perturbation B does not create the bound states higher than $m_{1,2}$ very efficiently. It is significant to set up the perturbation operator, which does not commute with any terms of the Hamiltonian. Note that the exact diagonalization method allows us to survey various types of the (off-diagonal) perturbation operators so as to observe $m_{3,4,\ldots}$ clearly.

3. Summary and discussions

The hierarchy $m_{2,3,4}/m_1$ for the $(2+1)$-dimensional $q = 3$ Potts model (8) was investigated with the numerical diagonalization method. The method allows us to calculate the dynamical susceptibilities $\chi''_{A,B}$, Eqs. (12) and (17), via the continued-fraction expansion [28]. Through the probe χ''_A, we obtained $(m_2/m_1, m_3/m_1, m_4/m_1) = [1.80(3), 2.5(1), 3.05(25)]$. The particles $m_{3,4}$ acquire intrinsic peak widths, $\Delta m_3/m_1 = 0.3$ and $\Delta m_4/m_1 = 0.35$, respectively; these spectra are embedded within the two-magnon spectrum. According to

Refs. [18, 19], the hierarchy $m_{2,3,4}/m_1$ of the Potts model and that of the pure gauge theory are alike. For instance, as for the Z_2-symmetric gauge group [36], there was reported a hierarchy, $(m_{(0^+)'}/m_{0^+}, m_{(0^+)''}/m_{0^+}, m_{(2^+)'}/m_{0^+}) = [1.88(2), 2.59(4), 3.23(7)]$, quite reminiscent of ours, Eq. (16).

As a reference, we calculated χ''_B (17); here, the operator B coincides with the second term of the Hamiltonian (8), and hence, it would be relevant to the experimental study. It turned out that the probe χ''_B is insensitive to the hierarchy $m_{3,4,\ldots}$, indicating that the choice of the perturbation operator is vital to observe $m_{3,4,\ldots}$. In this sense, the exact diagonalization method has an advantage in that we are able to treat various perturbation operators so as to observe the hierarchy $m_{3,4,\ldots}$ clearly.

Acknowledgment

This work was supported by a Grant-in-Aid for Scientific Research (C) from Japan Society for the Promotion of Science (Grant No. 25400402).

References

References

[1] A.B. Zamolodchikov, Int. J. Mod. Phys. A **3** (1988) 743.

[2] G. Delfino, J. Phys. A **37** (2004) R45.

[3] P. Fonseca and A. Zamolodchikov, J. Stat. Phys. **110** (2003) 527.

[4] R. Coldea, D. A. Tennant, E. M. Wheeler, E. Wawrzynska, D. Prabhakaran, M. Telling, K. Habicht, P. Smeibidl, and K. Kiefer, Science **327** (2010) 177.

[5] M. Caselle, M. Hasenbusch, and P. Provero, Nucl. Phys. B **556** (1999) 575.

[6] D. Lee, N. Salwen, and M. Windoloski, Phys. Lett. B **502** (2001) 329.

[7] M. Caselle, M. Hasenbusch, P. Provero, and K. Zarembo, Nucl. Phys. B **623** (2002) 474.

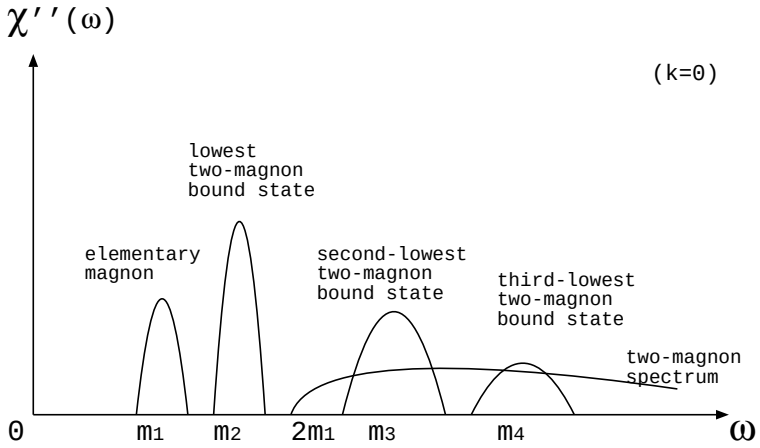

Figure 1: A schematic drawing of a dynamical susceptibility for the Potts model (8) in the ordered phase within the zero-momentum ($k = 0$) sector is presented. There appear hierarchical peaks with the mass gaps $m_{1,2,\ldots}$: The elementary excitation m_1 corresponds to the single magnon, which forms a series of bound states $m_{2,3,\ldots}$. The two-magnon spectrum extends above $\omega > 2m_1$. The excitations $m_{1,2,\ldots}$ may have a relevance to the glueball spectrum for the (pure) gauge field theory [18, 19].

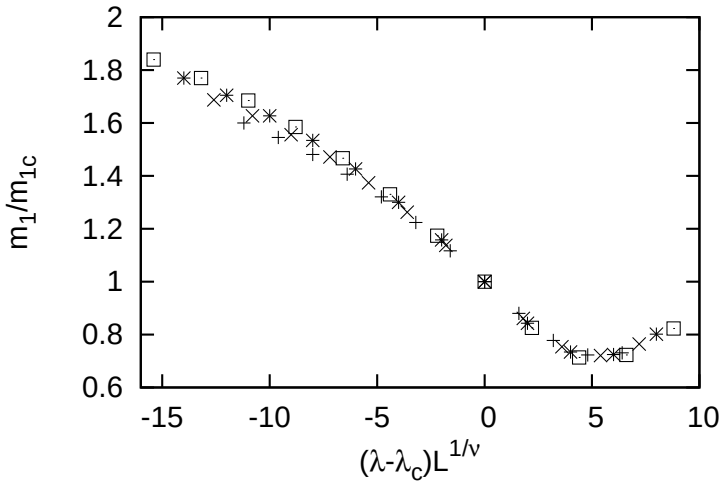

Figure 2: The scaling plot, $(\lambda - \lambda_c)L^{1/\nu}$-$m_1/m_{1c}$, is presented for (+) $N = 16$, (×) 18, (∗) 20, and (□) 22; here, we adopted the scaling theory [26, 31] for the first-order phase transition. The scaling parameters, $\lambda_c = 0.8758$ and $\nu = 0.5$, are taken from the existing literatures, Refs. [25] and [26, 31], respectively; namely, there is no adjustable parameter involved in the scaling analysis.

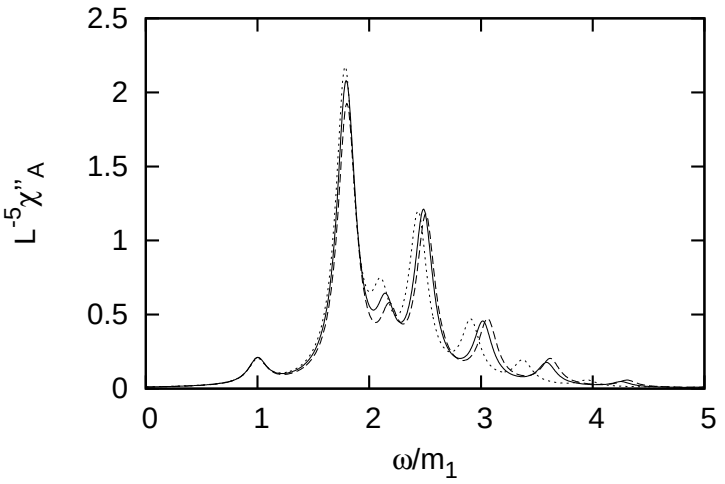

Figure 3: The scaling plot, ω/m_1-$L^{-5}\chi''_A(\omega)$, is presented with fixed $(\lambda-\lambda_c)L^{1/\nu}=-4$ and $\eta=0.1m_1$ for various $N=18$ (dotted), 20 (solid), and 22 (dashed); the scaling parameters, λ_c and ν, are the same as those of Fig. 2. The signals, $\omega/m_1\approx 1.8$, 2.5 and 3, correspond to the $m_{2,3,4}$ particles, respectively; see text for details.

[8] Y. Nishiyama, Phys. Rev. E **77** (2008) 051112.

[9] S. Dusuel, M. Kamfor, K. P. Schmidt, R. Thomale, and J. Vidal, Phys. Rev. B **81** (2010) 064412.

[10] Y. Nishiyama, Physica A **413** (2014) 577.

[11] F. Rose, F. Benitez, F. Léonard, and B. Delamotte, Phys. Rev. D **93** (2016) 125018.

[12] Y. Nishiyama, Physica A **463** (2016) 303.

[13] L. Chim and A. Zamolodchikov, Int. J. Mod. Phys. A **7** (1992) 5317.

[14] G. Delfino, Nucl. Phys. B **791** (2008) 265.

[15] L. Lepori, G. Z. Tóth and G. Delfino, J. Stat. Mech.: Theory and Experiment (2009) P11007.

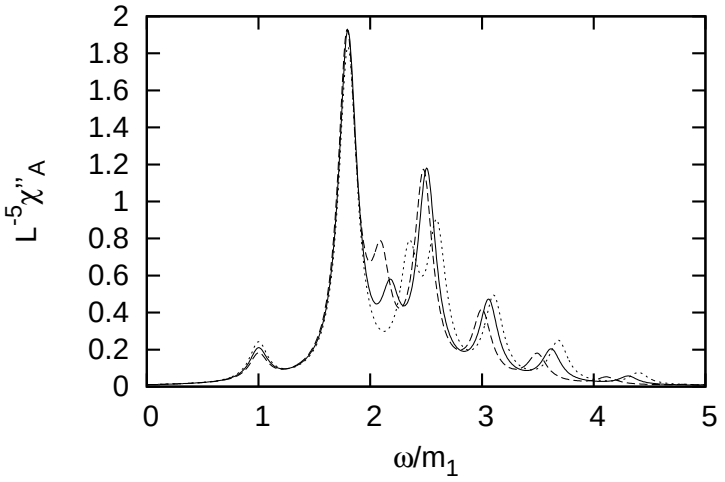

Figure 4: The scaling plot, ω/m_1-$L^{-5}\chi''_A(\omega)$, is presented with fixed $N = 22$ and $\eta = 0.1m_1$ for various values of the scaling parameter, $(\lambda - \lambda_c)L^{1/\nu} = -3$ (dotted), -4 (solid), and -5 (dashed); the scaling parameters, λ_c and ν, are the same as those of Fig. 2. Because the scaling parameter $(\lambda - \lambda_c)L^{1/\nu}$ is raging, the curves do not necessarily overlap. The peak position seems to be invariant, albeit with varying the scaling parameter, indicating that each scaled mass $m_{2,3,\ldots}/m_1$ takes a constant value in proximity to the transition point.

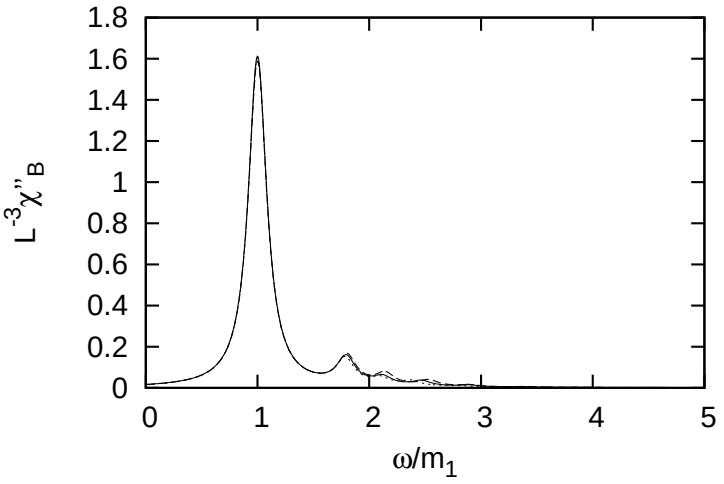

Figure 5: The scaling plot, ω/m_1-$L^{-3}\chi''_B(\omega)$, is presented with fixed $(\lambda-\lambda_c)L^{1/\nu}=-4$ and $\eta=0.1m_1$ for various $N=18$ (dotted), 20 (solid), and 22 (dashed); the scaling parameters, λ_c and ν, are the same as those of Fig. 2. A faint signal around $\omega/m_1\approx 2$ is attributed to the two-magnon-spectrum threshold. The spectral weights for χ''_B differ significantly from those for χ''_A.

[16] S. B. Rutkevich, J. Stat. Mech.: Theory and Experiment (2015) P01010.

[17] M. Lencsés and G. Takács, J. High Energy Phys. **09** (2015) 146.

[18] R. Falcone, R. Fiore, M. Gravina and A. Papa, Nucl. Phys. B **767** (2007) 385.

[19] R. Falcone, R. Fiore, M. Gravina and A. Papa, Nucl. Phys. B **785** (2007) 19.

[20] F. J. Wegner, J. Math. Phys. **12** (1971) 2259.

[21] R. Balian, J. M. Drouffe and C. Itzykson, Phys. Rev. D **11** (1975) 2098.

[22] E. Fradkin and L. Susskind, Phys. Rev. D **17** (1978) 2637.

[23] B. Svetitsky and L. G. Yaffe, Nucl. Phys. B **210** (1982) 423.

[24] A. Athenodorou, R. Lau and M. Teper, Phys. Lett. B **749** (2015) 448.

[25] C. J. Hamer, J. Oitmaa and Z. Weihong, J. Phys. A: Math. and Gen. **25** (1992) 1821.

[26] C. J. Hamer, M. Aydin, J. Oitmaa and H.-X. He, J. Phys. A: Math. Gen. **23** (1990) 4025.

[27] Y.-W. Dai, S. Y. Cho, M. T. Batchelor and H.-Q. Zhou, Phys. Rev. E **89** (2014) 062142.

[28] E. R. Gagliano and C. A. Balseiro, Phys. Rev. Lett. **59** (1987) 2999.

[29] M. E. Fisher and A. N. Berker, Phys. Rev. B **26** (1982) 2507.

[30] M. S. S. Challa, D. P. Landau and K. Binder, Phys. Rev. B **34** (1986) 1841.

[31] M. Campostrini, J. Nespolo, A. Pelissetto and E. Vicari, Phys. Rev. E **91** (2015) 052103.

[32] M. Campostrini, J. Nespolo, A. Pelissetto and E. Vicari, Phys. Rev. Lett. **113** (2014) 070402.

[33] M.A. Novotny, J. Appl. Phys. **67** (1990) 5448.

[34] Y. Nishiyama, Phys. Rev. E **78** (2008) 021135.

[35] D. Podolsky and S. Sachdev, Phys. Rev. B **86** (2012) 054508.

[36] V. Agostini, G. Carlino, M. Caselle and M. Hasenbusch, Nucl. Phys. B **484** (1997) 331.

[37] R. Fiore, A. Papa and P. Provero, Nucl. Phys. B Proc. Suppl. **119** (2003) 490.